Science AAAS

Negative Refraction at Visible Frequencies
Henri J. Lezec, *et al.*
Science **316**, 430 (2007);
DOI: 10.1126/science.1139266

Negative Refraction at Visible Frequencies

Henri J. Lezec,[1,2]*† Jennifer A. Dionne,[1]* Harry A. Atwater[1]

Nanofabricated photonic materials offer opportunities for crafting the propagation and dispersion of light in matter. We demonstrate an experimental realization of a two-dimensional negative-index material in the blue-green region of the visible spectrum, substantiated by direct geometric visualization of negative refraction. Negative indices were achieved with the use of an ultrathin Au-Si_3N_4-Ag waveguide sustaining a surface plasmon polariton mode with antiparallel group and phase velocities. All-angle negative refraction was observed at the interface between this bimetal waveguide and a conventional Ag-Si_3N_4-Ag slot waveguide. The results may enable the development of practical negative-index optical designs in the visible regime.

When a beam of light enters a material from vacuum or air at non-normal incidence, it undergoes refraction—a change in its direction of propagation. The angle of refraction depends on the absolute value of the refractive index of the medium, according to Snell's law. For all naturally occurring substances, the beam is deflected to the opposite side of the interface normal, and the refractive index is taken to be positive.

In 1968, Veselago studied a theoretical material with simultaneously negative electric permittivity ε and magnetic permeability μ, and predicted that it would have a negative index of refraction *n* (*1*). Light crossing the boundary between such a medium and one with a positive refractive index would refract to the same side of the normal. Such a deflection, termed negative refraction, was predicted to lead to a variety of enabling applications, most notably subwavelength focusing with resolution well below the diffraction limit (*2*).

Considerable research has been devoted to developing artificial electromagnetic media with negative *n* resulting from negative ε and μ (*3*, *4*). Such media, known as negative-index materials (NIMs), were first implemented at microwave frequencies on the order of 10 GHz by means of periodic assemblies of millimeter-scale split-ring resonators and wires (*5*, *6*). Negative values of μ and ε were simultaneously achieved via, respectively, the resonant capacitive-inductive response of the split-rings (*7*) and the effective plasma response of the wire lattice determined by mutual inductance (*8*). All-angle negative refraction in two dimensions was then demonstrated by direct observation of plane-wave refraction through prism-shaped segments of such assemblies (*5*, *6*).

Efforts are now directed toward scaling down NIMs for operation at optical frequencies (*9*, *10*). So far, structures have been limited to one (*11*–*14*) or a few (*15*) layers of discrete resonator elements. Transmission and reflection spectra measured with out-of-plane illumination enable retrieval of ε, μ, and *n* (*16*); in this manner, negative indices were inferred at infrared frequencies (*11*–*13*, *15*) and recently at the red end of the visible spectrum (*14*). However, because the thickness of such NIMs is substantially smaller than the free-space wavelength, the interaction volume with the incident radiation presumably remains too small to induce angular deviations of light with sufficient amplitude to provide direct evidence of negative refraction.

Here, we demonstrate a planar NIM at visible frequencies. It is based on the proposal that a suitably designed metal-insulator-metal (MIM) waveguide can act as a two-dimensional NIM characterized by an effective ε and μ that are both negative when averaged over the thickness of the waveguide (*17*–*21*). The negative response arises from the in-plane isotropic dispersion properties of a transverse magnetic (TM) mode involving coupled surface plasmon polaritons (SPPs) at each metal-dielectric interface. For frequencies above the surface plasmon resonance frequency ω_{SP}, but below the bulk plasmon frequency ω_P, the dispersion curve exhibits negative slope leading to antiparallel group and phase velocities, meaning that the energy and phase fronts propagate in opposite directions. Such a mode then behaves as if it had a negative index of refraction (*22*). If it is the only sustained mode, this index can be considered to be equivalent to the effective index of refraction of the two-dimensional medium itself.

In this experiment, we used two MIM waveguides cascaded in series to directly visualize negative refraction. The first waveguide is designed to sustain propagation of only a single negative-index mode over a broad subset of the visible frequency range. The second waveguide is tailored to sustain propagation of only positive-index modes over the same range. Structures are fabricated by applying a sequence of thermal evaporation and focused ion beam milling steps to both sides of a suspended Si_3N_4 membrane.

Figure 1A illustrates the dispersion properties of a planar Ag-Si_3N_4-Ag waveguide with dielectric core thickness t = 500 nm. Modal properties were calculated via numerical solution of Maxwell's equations assuming perfect coupling between each metal-dielectric interface (*23*, *24*). The waveguide sustains a number of TM modes (*25*), each identified with the closest related mode of a parallel-plate waveguide with perfect metal surfaces (*26*). Most modes lie to the left of the light line $\omega = ck_0/n_d$, where n_d is the refractive index of the core and $k_0 = 2\pi/\lambda_0$. These "photonic" modes are characterized by a propagation constant $\beta < n_d k_0$. In addition, an SPP mode characterized by $\beta > n_d k_0$ and corresponding to degenerate, cutoff-free TM_0 and TM_1 modes is present to the right of the light line. Over the entire visible range (400 nm < λ_0 < 700 nm), all allowed modes obey the condition $d\omega/d\beta \geq 0$, corresponding to a positive refractive index of light in the waveguide.

As the dielectric core thickness t is reduced, the cutoff energy of each photonic mode increases. For t = 50 nm, a single allowed mode remains in the visible range: the TM_0 SPP mode [the TM_1 SPP mode of Fig. 1A is completely attenuated by absorption (*24*)]. The dispersion curve of this mode (Fig. 1B, gray curve) exhibits a negative slope ($d\omega/d\beta < 0$) and hence negative-index behavior over the ultraviolet frequency range $\omega_{SP}^{Ag\text{-}Si_3N_4} < \omega < \omega_P^{Ag}$ (where $\omega_{SP}^{Ag\text{-}Si_3N_4}$ and ω_P^{Ag} are the resonant frequencies of the Ag-Si_3N_4 surface plasmon and the Ag bulk plas-

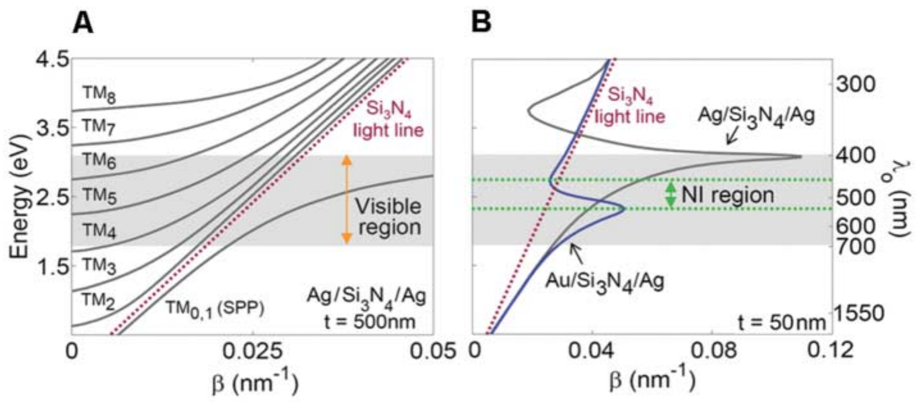

Fig. 1. Implementation of positive- and negative-index MIM waveguides. (**A**) Calculated dispersion curves for an Ag-Si_3N_4-Ag waveguide with a dielectric core thickness t = 500 nm. (**B**) Calculated dispersion curves for Ag-Si_3N_4-Ag and Au-Si_3N_4-Ag waveguides with t = 50 nm.

[1]Thomas J. Watson Laboratory of Applied Physics, California Institute of Technology, Pasadena, CA 91125, USA. [2]Centre National de la Recherche Scientifique, 3 rue Michel-Ange, 75794 Paris Cedex 16, France.

*These authors contributed equally to this work.
†To whom correspondence should be addressed. E-mail: lezec@caltech.edu

mon, respectively). By swapping Ag with Au in one of the cladding layers, this region of negative slope can be shifted to the interval 470 nm < λ_0 < 530 nm, well within the visible (Fig. 1B, blue curve). Calculated losses for the resulting negative-index mode in this Au-Si_3N_4-Ag waveguide indicate a characteristic power attenuation distance of ~50 nm, as well as an average figure of merit FOM = |Re(n)/Im(n)| ~ 4. This FOM appears somewhat higher than those summarized (*9*, *10*) for recent resonator-based negative-index metamaterials operating at the onset between the visible and infrared regimes (where quoted FOMs range from 3 at λ_0 = 1.4 μm to 0.5 at λ_0 = 780 nm).

Figure 2A displays a cross section of the experimental device used to demonstrate negative refraction. An Au-Si_3N_4-Ag waveguide (W1) with a thin dielectric core (t_1 = 50 nm) is positioned between two identical Ag-Si_3N_4-Ag waveguides (W2) with thick dielectric cores (t_2 = 500 nm). The 100-nm thicknesses of the Ag and Au cladding layers are substantially larger than the mode skin depth (*27*). In addition, a 200-nm-thick layer of Al is deposited on each side of the waveguide to ensure complete opacity of the respective top and bottom cladding layers. Slits of subwavelength width (w = 400 nm) couple light into and out of the waveguide (*28*). The input slit is illuminated at normal incidence with TM-polarized laser light (H-field parallel to the slit). The output slit is imaged using a 50× objective coupled to a liquid nitrogen–cooled charge-coupled device camera.

Direct characterization of positive or negative refraction is achieved by shaping W1 into a prism in the plane of propagation (Fig. 2B). A guided mode is first launched in W2 via the input slit. This mode impinges at normal incidence on the leading edge of the prism, where it excites a SPP mode that propagates through W1 with effective index n_1. The SPP mode in turn impinges on the slanted interface between W1 and W2, at angle φ_1. The mode is then refracted at an angle φ_2 into a guided mode of W2 with effective index n_2. We estimate φ_2 from the projected position of the mode on the output slit and use Snell's law (*22*) to determine the ratio $n_1/n_2 = \sin(\varphi_2)/\sin(\varphi_1)$.

Refraction results obtained at wavelengths λ_0 = 685 nm and 514 nm are illustrated in Fig. 3. These two wavelengths fall, respectively, in the calculated positive- and negative-index regions of W1 (Fig. 1B).

Figure 3A evaluates waveguide transmission through W2 in the absence of a prism. At both wavelengths, a clear image of the input slit is projected onto the output slit, consistent with previous observations of low lateral mode divergence within MIM waveguides (*28*).

Figure 3B illustrates the effect of introducing two symmetric prisms of W1 into W2. The diagonal edges of both prisms are parallel and form an angle of 7° with respect to the wavefront launched by the input slit. Vertical displacement of the incident beam is proportional to the angle

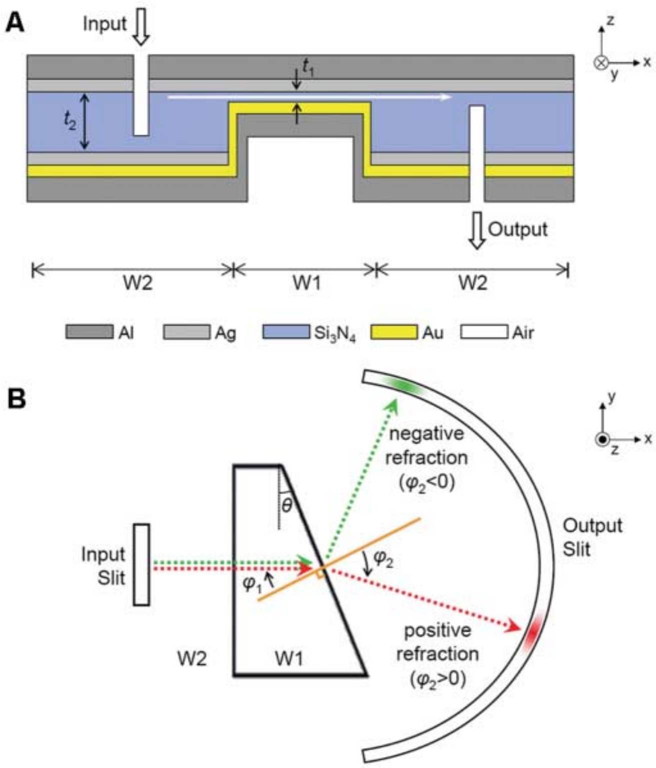

Fig. 2. Schematic diagram of structure fabricated to demonstrate in-plane negative refraction. A prism-shaped segment of Au-Si_3N_4-Ag waveguide with variable dielectric core thickness t_1 and edge angle θ ("W1") is embedded in an Ag-Si_3N_4-Ag waveguide of fixed core thickness t_2 = 500 nm ("W2"). Two slits extending into the waveguide core (nominal width w = 400 nm) are used to excite and intercept, respectively, a guided electromagnetic mode. (**A**) Cross section showing path of light through structure (white arrows). (**B**) Corresponding plan view showing hypothetical path of guided mode at two different frequencies illustrating, respectively, positive refraction (red arrow) and negative refraction (green arrow).

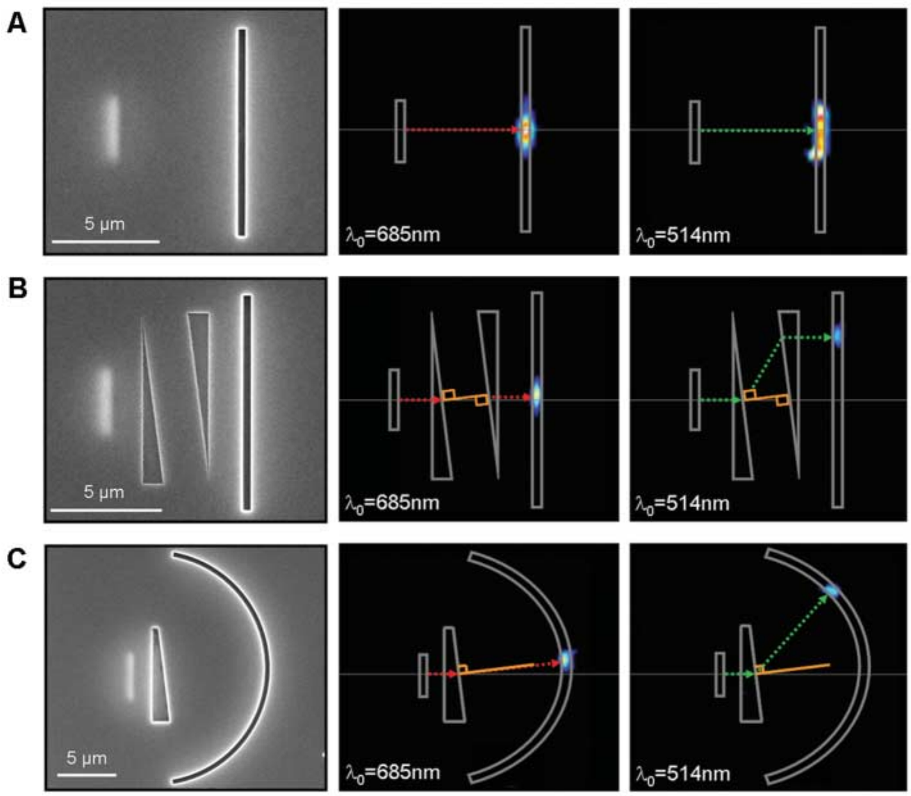

Fig. 3. Direct visualization of in-plane negative refraction. Three waveguide configurations are explored: (**A**) W2 alone, (**B**) two prisms of W1 (t_1 = 50 nm, θ = 7°) embedded in W2, and (**C**) one prism of W1 (t_1 = 50 nm, θ = 7°) embedded in W2. Left column: Scanning electron micrograph image of output side. Input slit position is revealed by electron transparency. Center and right columns: Optical microscope image of output side, given input-side illumination at λ_0 = 685 nm and 514 nm, respectively.

of refraction at the first angled interface, φ_2. The double-prism configuration corrects for differences in the optical path length, ensuring that the mode experiences uniform absorption during its transit from input slit to output slit. At λ_0 = 685 nm, the observed output-spot position indicates positive refraction at both slanted interfaces between W1 and W2, with an angle φ_2 = +0.1°. In contrast, at λ_0 = 514 nm, the output-spot position indicates negative refraction between W1 and W2, with an angle φ_2 = –51°. Given the prism angle $\varphi_1 = \theta$ = 7°, Snell's law yields an index ratio n_1/n_2 = +0.01 and –6.26 at λ_0 = 685 nm and 514 nm, respectively.

Similar trends are observed when a single prism of W1 is placed in the path of the guided mode in W2 (Fig. 3C). The straight output slit of Fig. 3B is replaced with a semicircular slit to ensure that the refracted mode intersects the slit at normal incidence for any refraction angle. At λ_0 = 685 nm, the position of the output spot indicates positive refraction at the interface between W1 and W2, with an angle φ_2 = +0.1°. When λ_0 is reduced to 514 nm, the output-spot position shifts, indicating negative refraction at the interface between W1 and W2, with an angle φ_2 = –43.7°. Given the incident angle φ_1 = 7°, Snell's law yields an index ratio n_1/n_2 = +0.01 and –5.57 at λ_0 = 685 nm and 514 nm, respectively. These values are in good agreement with those measured using the double-prism configuration of Fig. 3B.

To derive the mode index of the thin Au-Si_3N_4-Ag waveguide, n_1, it is necessary to determine the mode index of the surrounding thicker Ag-Si_3N_4-Ag waveguide, n_2. To circumvent the difficulty of estimating n_2 theoretically, given the prediction of multimodal dispersion properties for W2 (Fig. 1A), we measured n_2 directly by an interferometric technique (*22*). At λ_0 = 514 nm, we obtained n_2 = 0.82, which implies effective refractive indices for the Au-Si_3N_4-Ag waveguides of Fig. 3 that are both large and negative: n_1 = –4.6 and –5.1 for Fig. 3, B and C, respectively. At λ_0 = 685 nm, we measured n_2 = 0.75, yielding a very small positive index n_1 = 0.01 in both cases. The effective index n_1 of a number of prisms with different angles θ and dielectric core thicknesses t_1 is summarized in Fig. 4A; data are tabulated for closely spaced free-space wavelengths spanning the predicted negative-index region. In particular, the relative invariance of n_1 as a function of θ confirms that our structures indeed obey all-angle in-plane refraction according to Snell's law (*22*). Finally, we plotted the full set of refraction data $n_1(\lambda)$ as $\lambda(\beta)$, yielding the dispersion behavior of the guided mode in the prism (Fig. 4B); the dispersion curve clearly presents a negative slope for λ_0 between 476 and 514 nm, in good agreement with calculations.

Using specially tailored metal-insulator-metal waveguides, we have realized a planar material with an effective negative refractive index in the blue-green region of the visible spectrum. Isotropic negative refraction in two dimensions is directly observed; in resonator-based metamaterials, such a measurement has so far been achieved only in the microwave regime. Nonresonant negative-index behavior is achieved over a broad ~50-nm (~λ_0/10) wavelength range, which can in principle be further extended by increasing the dielectric constant of the waveguide core. The structure is straightforward to fabricate because its performance depends only on the plasmonic properties of two smooth metal-dielectric interfaces and a single critical dimension adjusted to ensure monomode behavior: the thickness of a silicon nitride film. The approach appears promising for straightforward two-dimensional implementation of theoretically predicted negative refraction–based devices, such as a perfect lens capable of nonquasistatic, far-field focusing with subwavelength resolution (*2*). In addition, the inherent simplicity of the structure hints at its potential as a building block for future artificial media capable of all-angle negative refraction in three dimensions (*18*, *19*).

A

	Single Prism				Double Prism
t_1 (nm) →	150	150	75	50	50
λ_0(nm) ↓	□	■	▲	○	●
514	-3.79	-3.85	-4.65	-4.57	-5.14
501	-2.49	-2.52	-2.72		
496	-1.82	-1.81	-2.02		
488	-1.84	-1.71	-2.09		
476	-1.07	-1.18	-1.38		
	θ=5°	θ=7°			

B

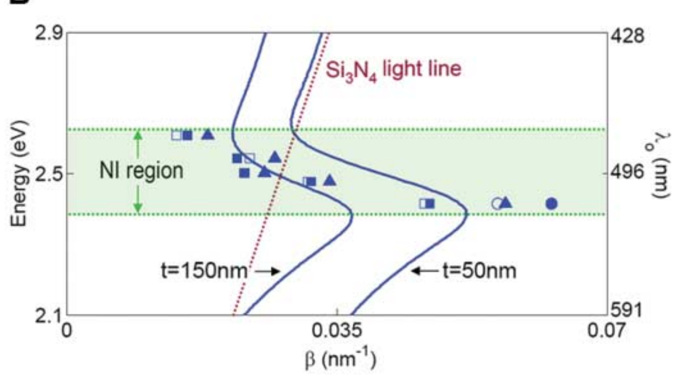

Fig. 4. Measured mode index (**A**) and mode dispersion (**B**) of Au-Si_3N_4-Ag prisms with various values of t_1 and θ, for frequencies spanning the negative-index region. The calculated dispersion curves for limiting cases *t* = 150 nm and *t* = 50 nm are also included.

References and Notes

1. V. G. Veselago, *Sov. Phys. Usp.* **10**, 509 (1968).
2. J. B. Pendry, *Phys. Rev. Lett.* **85**, 3966 (2000).
3. S. A. Ramakrishna, *Rep. Prog. Phys.* **68**, 449 (2005).
4. C. M. Soukoulis, M. Kafesaki, E. N. Economou, *Adv. Mater.* **18**, 1941 (2006).
5. R. A. Shelby, D. R. Smith, S. Schultz, *Science* **292**, 77 (2001).
6. A. A. Houck, J. B. Brock, I. L. Chuang, *Phys. Rev. Lett.* **90**, 137401 (2003).
7. J. B. Pendry, A. J. Holden, D. J. Robbins, W. J. Stewart, *IEEE Trans. Microw. Theory Tech.* **47**, 2075 (1999).
8. J. B. Pendry, A. J. Holden, W. J. Stewart, I. Youngs, *Phys. Rev. Lett.* **76**, 4773 (1996).
9. V. Shalaev, *Nat. Photonics* **1**, 41 (2007).
10. C. M. Soukoulis, S. Linden, M. Wegener, *Science* **315**, 47 (2007).
11. S. Zhang *et al.*, *Phys. Rev. Lett.* **95**, 137404 (2005).
12. V. M. Shalaev, *Opt. Lett.* **30**, 3356 (2005).
13. G. Dolling, C. Enkrich, M. Wegener, C. M. Soukoulis, S. Linden, *Science* **312**, 892 (2006).
14. G. Dolling, M. Wegener, C. M. Soukoulis, S. Linden, *Opt. Lett.* **32**, 53 (2007).
15. G. Dolling, M. Wegener, S. Linden, *Opt. Lett.* **32**, 551 (2007).
16. D. R. Smith, S. Schultz, P. Markos, C. M. Soukoulis, *Phys. Rev. B* **65**, 195104 (2002).
17. P. Tournois, V. Laude, *Opt. Commun.* **137**, 41 (1997).
18. G. Shvets, *Physica B* **338**, 338 (2003).
19. G. Shvets, *Phys. Rev. B* **67**, 035109 (2003).
20. A. Alu, N. Engheta, *J. Opt. Soc. Am. B* **23**, 571 (2006).
21. H. Shin, S. H. Fan, *Phys. Rev. Lett.* **96**, 073907 (2006).
22. See supporting material on *Science* Online.
23. J. A. Dionne, L. A. Sweatlock, H. A. Atwater, A. Polman, *Phys. Rev. B* **72**, 075405 (2005).
24. J. A. Dionne, L. A. Sweatlock, H. A. Atwater, A. Polman, *Phys. Rev. B* **73**, 035407 (2006).
25. Transverse electric (TE) modes also exist but are not excited given the incident polarization.
26. K. Y. Kim, Y. K. Cho, H. S. Tae, J. H. Lee, *Opt. Express* **14**, 320330 (2006).
27. For 470 nm < λ_0 < 530 nm, calculated skin depths in the Ag and Au layers do not exceed 21.5 nm and 30.0 nm, respectively.
28. J. A. Dionne, H. J. Lezec, H. A. Atwater, *Nano Lett.* **6**, 1928 (2006).

29. Supported by a National Defense Science and Engineering Graduate Fellowship administered by the Army Research Office (J.A.D.) and by the Air Force Office of Scientific Research under Plasmon Multidisciplinary University Research Initiative FA9550-04-1-0434. We thank L. Sweatlock, D. Pacifici, R. Walters, B. Kayes, N. Vu, G. Derose, and A. Scherer for engaging discussions and technical assistance.

Supporting Online Material

www.sciencemag.org/cgi/content/full/1139266/DC1
SOM Text
Figs. S1 and S2
References

26 December 2006; accepted 12 March 2007
Published online 22 March 2007;
10.1126/science.1139266
Include this information when citing this paper.